Characterization of Dielectric Charging in MEMS Using Diffusive Representation

Maria-Teresa Atienza, Sergi Gorreta, *Student Member*, *IEEE*, Joan Pons-Nin and Manuel Dominguez-Pumar, *Senior Member*, *IEEE*

***Abstract*—This paper introduces Diffusive Representation as a novel approach to characterize the dynamics of charge trapped in dielectric layers of microelectromechanical systems (MEMS). Diffusive Representation provides a computationally efficient method to achieve an arbitrary order state-space model of the charging dynamics. This approach is particularly well suited to analyze the dynamics of the dielectric charge under non-trivial controls, as in the case of sliding mode controllers. The diffusive symbol of the experimental structure has been obtained from open-loop measurements, in which Pseudo Random Binary Sequences (PRBS) are applied to the device. The obtained model exhibits good agreement with experimental data and also allows to model the behaviour of the charge dynamics under excitation with arbitrary binary signals.**

***Index Terms*—Diffusive Representation, MEMS, dielectric charging**

I. Introduction

ELECTROSTATICALLY actuated MEMS devices have been used as varactors, resonators and switches in a large set of applications. Nevertheless, the parasitic charge trapped in the dielectric layers of these devices produces undesired effects such as pull-in voltage drift, capacitance-voltage $C(V)$ curve shifts or even stiction of moveable parts. This serious reliability problem still hinders the massive commercial use of these devices [1]. Accordingly, characterization of the charging dynamics is an important issue that has been studied using different methods. For instance, in [2] iterative measurements of pull-in voltage have been used to monitor the charge evolution with time. However, this strategy alters the amount of trapped charge and is not compatible with normal operation of the devices. In [3], the application of bipolar voltages allowed to monitor $C(V)$ shifts through quasi differential capacitance measurements. This method allows knowing the state of the charge without distorting the measurement nor affecting the normal operation of the device.

This paper improves the work introduced in [3], where the dynamics of the dielectric charge for the contactless case was described using a multi-exponential model. The parameters of this model were obtained with the unconstrained non-linear minimization Nelder–Mead algorithm. In this paper, however, the characterization method uses the Diffusive Representation technique, which is a suitable framework for any diffusive physical phenomenon [4], being even able to accurately describe fractional order models. The use of this type of models is appropiate since diffusion processes have been associated with dielectric charging in MEMS [5]. Furthermore, there is a link in [6] between fractional systems and the typically observed multiexponential or stretched-time exponential type responses [2], [7] usually found in dielectric charging.

These behavioural models are particularly useful in the analysis of dielectric charging control using the tools of sliding mode controllers [8]. Diffusive Representation has been widely used in thermal characterization [9] and dielectric polarization [4], [10], among others. Another key advantage of using Diffusive Representation is the reduction of the computational load respect other methods, as the model parameters are obtained with the linear least-squares method. This in particular allows to increase the model order if necessary, due to the fact that the identification problem is computationally tolerable.

II. Charge Characterization Method

This paper uses the voltage waveforms, or symbols BIT0 and BIT1, designed for charge characterization and control in [3], [8], [11], shown in Fig. 1. In BIT0, a negative voltage V^- is applied to the MEMS for a 'long' time $(1-\delta)T_s$, then positive voltage V^+ is applied for a 'short' time δT_s, being $\delta < 1$ and T_s the symbol duration. In BIT1, the same timing scheme but with opposite voltages is applied. During each symbol, the capacitance of the device is measured at times $(1-\delta)T_s$ and T_s. This allows obtaining a sample of the quasi-differential capacitance $\Delta C = C(V^+) - C(V^-) = C^+ - C^-$ at the end of each symbol. ΔC is related to the voltage shift of the $C(V)$, commonly defined as $V_{sh} = Q_d/C_d$, where Q_d and C_d are the total amount of charge trapped in the dielectric and the dielectric capacitance respectively. For devices working below pull-in a parabolic $C(V)$ shape can be considered. In this case the relationship between ΔC and V_{sh} is [11]:

$$\Delta C(t) = \alpha((V^+)^2 - (V^-)^2) - 2\alpha V_{sh}(t)(V^+ - V^-) \quad (1)$$

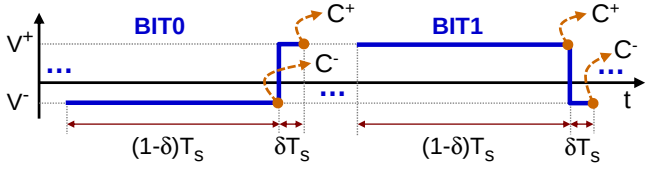

Fig. 1. Voltage waveforms, or symbols, for MEMS actuation and sensing. Capacitance measurements are performed at symbol times $(1-\delta)T_s$ and T_s.

Manuscript received April 5, 2016; revised July 25, 2016; accepted August 9, 2016. This work was supported in part by the Spanish Ministry MINECO under Projects TEC2013-48102-C2-1-P and FPI grant BES-2012-057618.

Micro and Nano Technologies Group, Universitat Politècnica de Catalunya, Barcelona, Spain. Corresponding author e-mail: maria.teresa.atienza@upc.edu.

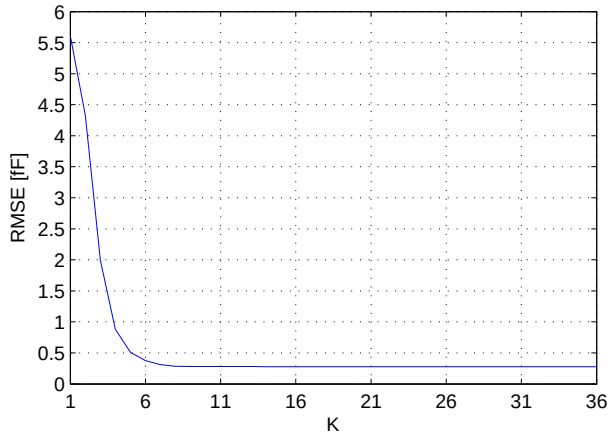

Fig. 2. Root Mean Square Error evolution of the fittings as a function of the model order K.

where α is the second order coefficient of the parabolic function.

In the MEMS used in the experiments of this work, applying BIT0 increases the amount of net dielectric charge Q_d, and thus the voltage shift V_{sh}, whereas applying BIT1 decreases both Q_d and V_{sh}.

III. Diffusive Representation

Diffusive Representation theory allows obtaining exact and approximate state realizations of a wide class of integral operators of rational or non-rational nature. This representation method, is an useful mathematical tool for any physical phenomena based on diffusion [4].

Given a non-rational transfer function, $H(p)$, associated with a convolution causal operator denoted by $H(\partial_t)$, the diffusive realization of this operator is expressed by the following input (u) – output (y) state space realization of $u \longmapsto y = H(\partial_t)u = h * u$ of the form [10]:

$$\begin{array}{lcl} \frac{\partial\psi(\xi,t)}{\partial t} & = & -\xi\psi(\xi,t) + u(t), \quad \psi(\xi,0) = 0 \\ y(t) & = & \int_0^\infty \eta(\xi)\psi(\xi,t)d\xi \end{array} \tag{2}$$

where $\xi \in \mathbb{R}$, $\eta(\xi)$ is the diffusive symbol of $H(\partial_t)$ and $\psi(\xi,t)$ is called the diffusive representation of $u(t) \in \{V^+, V^-\}$. The state-variable $\psi(\xi,t)$ is a time-frequency representation of the input only and is the solution to the differential equation of Eq. (2) [10]. The diffusive symbol $\eta(\xi)$ is a solution of Eq. (3) directly obtained from Laplace transform (with respect to t) [10].

$$H(j\omega) = \int_0^\infty \frac{\eta(\xi)}{j\omega + \xi} d\xi \quad \omega \in \mathbb{R} \tag{3}$$

The impulse response $h := \mathcal{L}^{-1}H$ can also be expressed from η: [10]

$$h(t) = \int_0^\infty e^{-\xi t}\eta(\xi)d\xi \tag{4}$$

and the diffusive symbol can be given also as the inverse Laplace transform of the impulse response: [10]

$$\eta = \mathcal{L}^{-1}h \tag{5}$$

In this paper we will consider that the charging dynamics associated with the application of two voltages, V^+ and V^-. This is described by the following equation that is equivalent to Eq. (2):

$$\begin{array}{lcl} \frac{\partial\psi(\xi,t)}{\partial t} & = & -\xi\psi(\xi,t) + \eta(\xi)^- \\ & + & (\eta(\xi)^+ - \eta(\xi)^-)\hat{u}(t), \quad \psi(\xi,0) = 0 \\ y(t) & = & \int_0^\infty \psi(\xi,t)d\xi \end{array} \tag{6}$$

where $\hat{u}(t) = \frac{u(t)-V^-}{V^+-V^-} \in \{1,0\}$ is the normalized input signal. $\eta(\xi)^+$ is the diffusive symbol associated with the actuation of the device with V^+ (when $\hat{u}=1$), while $\eta(\xi)^-$ is the diffusive symbol associated to V^- ($\hat{u}=0$).

A discrete approximation of $H(\partial_t)$ can be built discretizing the continuous variable ξ into $\{\xi_k\}_{1\le k\le K}$, where K is the order of the discretized model. This leads to an input – output approximation $u \longmapsto \tilde{y} \approx y = H(\frac{d}{dt})u$ of the form:

$$\begin{array}{lcl} \frac{d\psi_k(t)}{dt} & = & -\xi_k\psi_k(t) + \eta_k^- + \Delta\eta_k\hat{u}(t), \quad \psi_k(0) = 0 \\ \tilde{y}(t) & = & \sum_k^K \psi_k(t) \end{array} \tag{7}$$

where $\psi_k(t) = \psi(\xi_k,t)$, $\eta_k^\pm = \eta(\xi_k)^\pm$ and $\Delta\eta_k = (\eta_k^+ - \eta_k^-)$ for $k = 1, \cdots, K$.

If the first expression of Eq. (7) is splitted in two state variables, Eq. (8) is reached:

$$\begin{array}{lcl} \frac{d\psi_k^0(t)}{dt} & = & -\xi_k\psi_k^0(t) + 1, \qquad \psi_k^0(0) = 0 \\ \frac{d\psi_k^1(t)}{dt} & = & -\xi_k\psi_k^1(t) + \hat{u}(t), \quad \psi_k^1(0) = 0 \\ \tilde{y}(t) & = & \sum_k^K \eta_k^-\psi_k^0(t) + \sum_k^K \Delta\eta_k\psi_k^1(t) \end{array} \tag{8}$$

$\psi_k^0(t)$ and $\psi_k^1(t)$ are obtained after resolving the first and second differential equations from Eq. (8).

Given that the MEMS device can be charged at $t = t_0$, some coefficients, a_k, are added to the output $\tilde{y}(t)$ of the system which allow to 'forget' the initial conditions of the device. The third expression of Eq. (8) is then rewritten as:

$$\tilde{y}(t) = \sum_k^K \eta_k^-\psi_k^0(t) + \sum_k^K \Delta\eta_k\psi_k^1(t) + \sum_k^K a_k e^{-\xi_k(t-t_0)} \tag{9}$$

This step is necessary, since the device can be charged prior to starting the measurements and this may result in errors in the fitting procedure. The values of the coefficients are obtained together with the values of η_k^- and $\Delta\eta_k$ in the fitting of the experimental measurements.

The goodness of the approximation will depend on the chosen frequency mesh $\{\xi_k\}_{1\le k\le K}$, usually geometrically spaced in the band of interest and in concordance with the dynamic characteristics of the system [9]. The chosen bandwidth for ξ goes from $\xi_{min} = 2\pi/T$ to $\xi_{max} = \pi/2T_s$, where T is the total duration of the measurements (long enough for the stabilization of the system), and T_s is the sampling period. Therefore, the experiment duration and the sampling period set a limit on the minimum and maximum frequency respectively. It must be noted that, with a sufficiently dense frequency mesh it is possible to describe with arbitrary accuracy the response of any fractional system, therefore other types of response

can be very well approximated with DR [4], for example, stretched-time exponentials. The same also applies to the effect of an initial charging in the device, as in Eq. (9).

In particular, the objective of the identification problem is to infer the finite order diffusive symbols η_k^- and η_k^+ from experimental data. Let us assume a temporal mesh $[t_n]_{1\leq n\leq N} \in \mathbb{R}^+$, the matrix $\mathbf{A} = [[F_{n,k}]\ [G_{n,k}]\ [H_{n,k}]]$, where $F_{n,k} = \psi_k^0(t_n)$, $G_{n,k} = \psi_k^1(t_n)$ and $H_{n,k} = e^{-\xi_k(t_n - t_0)}$, and the vector $\hat{\boldsymbol{\eta}}^T = [[\eta_k^-]^T\ [\Delta\eta_k]^T\ [a_k]^T]$. Note that $\mathbf{F}, \mathbf{G}, \mathbf{H} \in \mathbb{R}^{N\times K}$ and $\boldsymbol{\eta}, \boldsymbol{\Delta\eta}, \mathbf{a} \in \mathbb{R}^K$. The solution to the identification problem is found solving the finite dimensional least-square problem formulated by [9]:

$$\min_{\eta\in\mathbb{R}^K} ||\mathbf{A}\hat{\boldsymbol{\eta}} - \mathbf{Y}||^2 \tag{10}$$

where $\mathbf{Y}$ is the output vector of the measurements, $\mathbf{Y}^T = \begin{bmatrix} y(t_0) & \dots & y(t_N) \end{bmatrix}$, being $y(t_n) = \Delta C(t_n)$ in our case. The solution to Eq. (10) is classically given by $\hat{\boldsymbol{\eta}} = [\mathbf{A}^*\mathbf{A}]^{-1}\mathbf{A}^*\mathbf{Y}$.

When resolving numerically the integral of Eq. (2), a logarithmic change of variable is necessary due to the fact that ξ variable is spaced geometrically. Specifically, $\xi = 10^x$ and $d\xi = (ln10)10^x dx$. Taking this into account, the second expression of the equation becomes:

$$y(t_n) = \int_{x_0}^{x_1} \eta(10^x)\psi(10^x, t) ln(10) 10^x dx \approx \sum_{k=1}^{K} \eta_k \psi_k(t_n)\lambda_k \tag{11}$$

The term λ_k divides the inferred diffusive symbols, $\eta_k = \frac{\hat{\eta}_k}{\lambda_k}$, where $\lambda_k = ln(10)log(r)\xi_k$ and r is the ratio of the geometric sequence of the mesh of ξ ($\xi_{k+1} = r\xi_k$).

IV. Experimental Results

The MEMS, fabricated with standard PolyMUMPS technology, is a two-parallel plate structure. The upper plate-electrode is a polysilicon layer, suspended over 2.75 μm of air gap, followed below by a 0.6 μm thick silicon nitride layer and the doped silicon substrate, which is the bottom electrode. The plate dimensions are 515x515 μm^2 and the pull-in voltage is around $14V$.

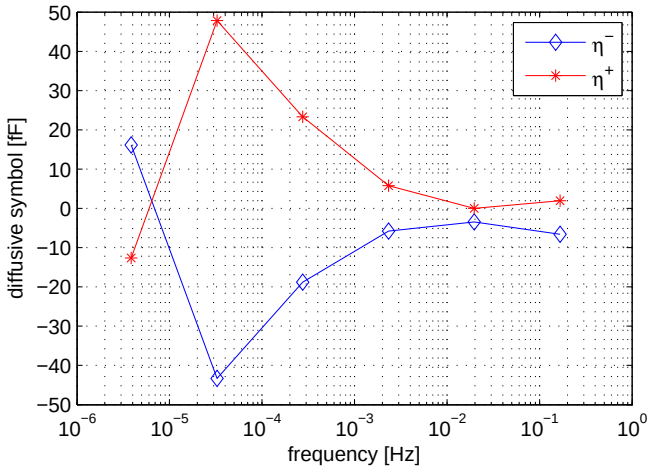

Fig. 3. 6-order diffusive symbols corresponding to the bipolar voltages V^- and V^+ resulting from pseudo-inversion of experimental measurements (model M1).

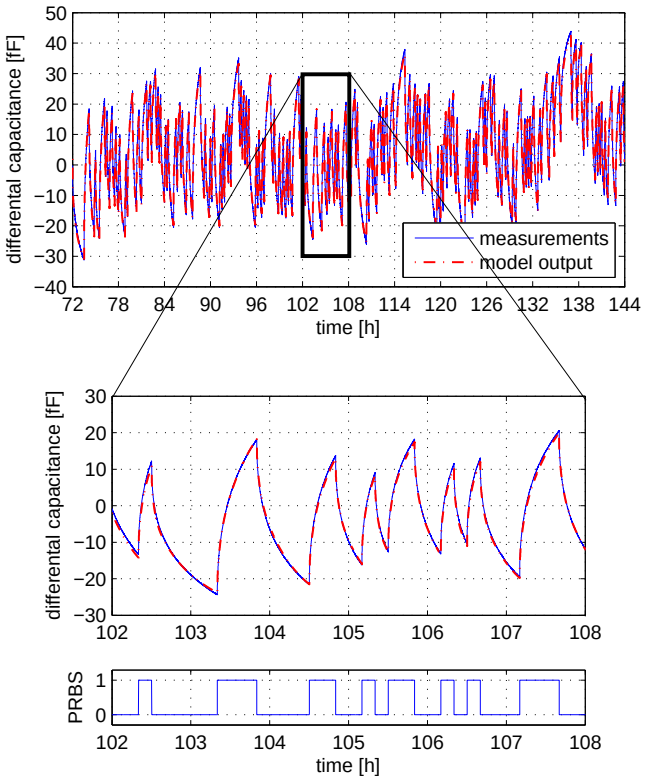

Fig. 4. Top: time evolution of the quasi differential capacitance from part II of the experiment (in blue) and the corresponding results obtained from model M1 from Fig. 3 (in red). Bottom: section between hours 102 and 108 of the time evolution of the experimental and the obtained data with the corresponding bit symbols applied to the MEMS in that period of time.

The device is actuated with BIT0 and BIT1 symbols following a specific pattern. The parameters of the symbols are $T_s = 1.5s$, $\delta = 1/3$, $\alpha = 1.4fF/V^2$ and $V^+ = -V^- = 5V$. The actuation pattern is a Pseudo Random Binary Sequence (PRBS), chosen because it has a wide spectrum and allows to improve the quality of the fittings in presence of noise [12].

A six-day experiment has been carried out. It is divided in two consecutive three-day parts as follows:

- **Part I**. For each PRBS symbol, '0's or '1's, either 40 BIT0 or 40 BIT1 waveforms are applied to the device. The total length of the PRBS sequence is 4320 symbols.
- **Part II**. For each PRBS symbol, 400 BIT0 or 400 BIT1 waveforms are applied to the device. Now, the length of the PRBS sequence, different to that of part I, is 432 symbols.

The data from each experiment has been processed separately and then compared to see if making an inference from the data of part I or part II results in different charging models. In the fitting process, some parameters are set. As both parts of the experiment have identical duration $T = 4320$ min and sampling period $T_s = 1.5s$, then the set of frequencies, ξ_k, range from $f_{min} = \frac{\xi_{min}}{2\pi} \approx 4\mu Hz$ to $f_{max} = \frac{\xi_{max}}{2\pi} \approx 0.1Hz$, and are geometrically spaced. It must be noted that the experiment should be adapted to the time scale desired in the

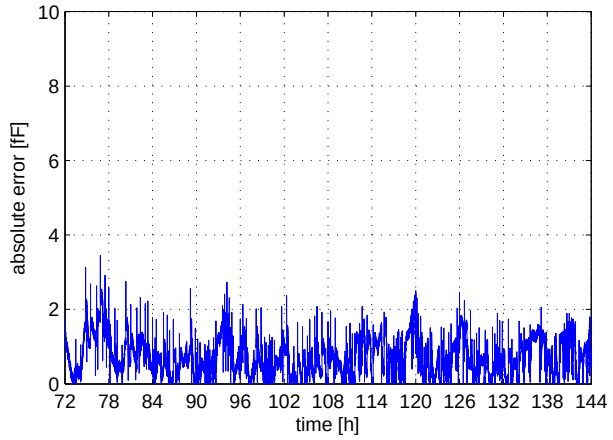

Fig. 5. Time evolution of the absolute error between measured quasi differential capacitance from part II of the experiment and the corresponding results obtained with model M1.

prediction capability of the model. This applies to the sampling frequency and the duration of the experiment.

The results of part I have been treated first. To determine which is the minimum model order that provides good adjustment to this experimental data, the evolution of the root mean square error (RMSE) of the fittings as a function of the model order has been analyzed. Figure 2 shows the evolution of the RMSE. As no substantial gain is achieved in terms of error beyond $K = 6$, this is the model order chosen (model M1). It has been observed that there is a good agreement between fittings and measurements. Figure 3 shows the diffusive symbols corresponding to the bipolar voltages applied to the device.

Secondly, the data of part II has been fitted using the same procedure as with data of part I to obtain model M2 and no noticeable difference is appreciated. The diffusive symbols obtained from the pseudo-inversion of the experimental data allow to model the dynamics of the charge trapped in the dielectric of the MEMS.

Finally, the input signal applied in part II has been fed into the model obtained from the measurements of part I (model M1). The objective is to compare the part II measurements with the results obtained with model M1. This is made in order to analyze the real capability of the DR models to describe the charging dynamics in real measurements. Figure (4) shows the quasi-differential measurements obtained during the experiment and the modeled data. The relationship between $\Delta C(t)$ and the total charge trapped in the dielectric of the MEMS, Q_d, is given in Eq. (1) [3], [8], [11]. To demonstrate the good matching between experimental and inferred data, Fig. (5) shows the time evolution of the absolute error, $|\Delta C_{meas}(t) - \Delta C_{model}(t)|$, along part II of the experiment. As it can be observed, the error is approximately constant over time.

V. Conclusion

A new method based on Diffusive Representation to characterize the dynamics of the parasitic charge trapped in the dielectric layer of MEMS devices has been presented. A dynamical finite-order model has been extracted from open-loop measurements using pseudo random binary sequences, which are useful in frequency domain system identification. The Diffusive Representation model agrees with the experimental data and has been successfully applied to model the behaviour of the charge dynamics of a real device. These state space models are very well suited to describe the behaviour of diffusive systems under non-trivial controls.

References

[1] W. M. V. Spengen, "Capacitive RF MEMS switch dielectric charging and reliability: a critical review with recommendations," *J. Micromech. Microeng.*, vol. 22, no. 7, p. 074001, Jun. 2012.

[2] M. Kouteoureli and G. Papaioannou, "The discharge current through the dielectric film in MEMS capacitive switches," in *European Microwave Integrated Circuits Conference (EuMIC)*, pp. 450–453, Oct. 2011.

[3] M. Dominguez-Pumar, S. Gorreta, J. Pons-Nin, E. Blokhina, P. Giounanlis, and O. Feely, "Real-time characterization of dielectric charging in contactless capacitive MEMS," *Analog Integr. Circuits Signal Process.*, vol. 82, no. 3, pp. 559–569, Mar. 2015.

[4] G. Montseny, *Representation diffusive*. Lavoisier, 2005.

[5] R. W. Herfst, P. G. Steeneken, J. Schmitz, A. J. G. Mank, and M. van Gils, "Kelvin probe study of laterally inhomogeneous dielectric charging and charge diffusion in rf mems capacitive switches," in *2008 IEEE International Reliability Physics Symposium*, pp. 492–495, Apr. 2008.

[6] H. Hara and Y. Tamura, "Dynamical process of complex systems and fractional differential equations," *Open Phys.*, vol. 11, no. 10, pp. 1238–1245, Oct. 2013.

[7] U. Zaghloul, G. J. Papaioannou, F. Coccetti, P. Pons, and R. Plana, "A systematic reliability investigation of the dielectric charging process in electrostatically actuated mems based on kelvin probe force microscopy," *J. Micromech. Microeng.*, vol. 20, no. 6, Jun. 2010.

[8] M. Dominguez-Pumar, S. Gorreta, and J. Pons-Nin, "Sliding-mode analysis of the dynamics of sigma-delta controls of dielectric charging," *IEEE Trans. Ind. Electron.*, vol. 63, no. 4, pp. 2320–2329, Apr. 2016.

[9] B. Allard, X. Jorda, P. Bidan, A. Rumeau, H. Morel, X. Perpina, M. Vellvehi, and S. M'Rad, "Reduced-Order Thermal Behavioral Model Based on Diffusive Representation," *IEEE Trans. Power Electron.*, vol. 24, no. 12, Dec. 2009.

[10] L. Laudebat, P. Bidan, and G. Montseny, "Modeling and optimal identification of pseudodifferential electrical dynamics by means of diffusive representation-part I: modeling," *IEEE Trans. Circuits Syst. I, Reg. Papers*, vol. 51, no. 9, pp. 1801–1813, Sept. 2004.

[11] S. Gorreta, J. Pons-Nin, E. Blokhina, O. Feely, and M. Dominguez-Pumar, "Delta-sigma control of dielectric charge for contactless capacitive MEMS," *J. Microelectromech. Syst*, vol. 23, no. 4, pp. 829–841, Aug. 2014.

[12] J. Davidson, D. Stone, M. Foster, and D. Gladwin, "Improved Bandwidth and Noise Resilience in Thermal Impedance Spectroscopy by Mixing PRBS Signals," *IEEE Trans. Power Electron.*, vol. 29, no. 9, Sept. 2014.